Shape phase transitions in the interacting boson model: Phenomenological versus microscopic descriptions

J. Kotila,[1,*] K. Nomura,[2,†] L. Guo,[3,4] N. Shimizu,[5] and T. Otsuka[2,5,6]

[1]*Center for Theoretical Physics, Sloane Physics Laboratory, Yale University, New Haven, Connecticut 06520-8120, USA*

[2]*Department of Physics, University of Tokyo, Hongo, Bunkyo-ku, Tokyo 113-0033, Japan*

[3]*College of Physical Sciences, Graduate University of Chinese Academy of Sciences, Beijing 100049, China*

[4]*RIKEN Nishina Center, Hirosawa, Wako-shi, Saitama 351-0198, Japan*

[5]*Center for Nuclear Study, University of Tokyo, Hongo, Bunkyo-ku, Tokyo 113-0033, Japan*

[6]*National Superconducting Cyclotron Laboratory, Michigan State University, East Lansing, Michigan 48824, USA*

(Received 30 March 2012; published 9 May 2012)

We investigate the shape phase transition in even-even $_{64}$Gd and $_{66}$Dy isotopes within the proton-neutron interacting boson model (IBM-2). The parameters of the IBM-2 Hamiltonian are fixed in two different ways: the usual phenomenological fitting calculation and the mapping of the constrained self-consistent mean-field calculation with a Skyrme energy density functional onto the appropriate boson system. Notable differences are found between the energy surfaces for the phenomenological and the mapped IBM-2. Key quantities for the collective structural evolution, including level energies, B(E2) values, quadrupole moments, and the two-neutron separation energies, are analyzed in comparison to the experimental data. We show that the transition in these quantities occurs rapidly with the neutron number in the IBM-2 phenomenology but is somewhat smeared out in the mapped IBM-2. The differences in the measurable quantities are consistent with what is suggested by the energy-surface analysis.

DOI: 10.1103/PhysRevC.85.054309 PACS number(s): 21.10.Re, 21.60.Ev, 21.60.Fw, 21.60.Jz

I. INTRODUCTION

Quantum phase transitions (QPTs) are one of the central issues in finite quantal systems, including atomic nuclei [1,2] and other mesoscopic systems such as atoms and polyatomic molecules [3,4], as well as in high-energy and condensed-matter physics. Particularly, equilibrium nuclear shape, e.g., of quadrupole type [5], undergoes a distinct structural evolution between spherical vibrational and deformed rotational states with the number of protons (Z) and/or neutrons (N). Here the nuclear QPT in this context means the one that occurs at a specific number of N and/or Z, which is discrete and as such should differ from the usual phase transition of thermodynamic type. As the QPT in nuclei is rather unique, it has drawn much attention from various perspectives (for a review, see Refs. [6,7], for instance).

Thanks to recent developments in experimental techniques, empirical study has revealed evidence of QPTs by looking at the various quantities: the varying 2_1^+ excitation energy, the rapid change in the ratio $R_{4/2} = E_x(4_1^+)/E_x(2_1^+)$, the evolution of the (spectroscopic) quadrupole moment for the 2_1^+ excited state, $Q_{2_1^+}$, and behavior of nucleon separation energies.

From the theoretical side, it has nowadays become possible to study nuclear QPT by means of fully microscopical models that start from (single) nucleonic motion and the driving nucleon-nucleon interactions in fermionic approaches, including self-consistent mean-field [8,9] and the large-scale shell-model [10] approaches. The former approach, for instance, gives a universal description of the nuclear intrinsic shape, while for the description of excited states one should go beyond the mean-field approximation to perform configuration mixing and/or restoration of broken symmetries. The calculation becomes, in general, much involved, particularly when triaxial degrees of freedom should be taken into account for medium-heavy and heavy nuclei. Along this line, nuclear QPT has been analyzed extensively using both nonrelativistic (e.g., Ref. [11]) and relativistic (e.g., Ref. [12]) energy density functionals.

Alternatively, phenomenological studies within the geometrical [13–15] and the algebraic [16] models provide measurable quantities in a computationally more moderate way. Particularly, the interacting boson model (IBM) [16] has been a well reputed example of algebraic models, and has in fact been quite successful in reproducing the low-lying structure of medium-heavy and heavy nuclei. Meanwhile, the microscopic derivation of the IBM Hamiltonian has been studied in terms of the shell model [17]. More recently three of the authors have proposed a way to determine the proton-neutron IBM (IBM-2) Hamiltonian through the mapping of the constrained energy surface, obtained from the standard self-consistent mean-field study using an energy density functional (EDF), onto the appropriate IBM-2 energy surface [18]. The vibrational-to-rotational transition in rare-earth nuclei has also been analyzed already in Refs. [19,20].

The first-order QPT, that is, the transition from spherical vibrational to axially deformed shapes, in the rare-earth region has been successfully analyzed within the IBM phenomenology (e.g., Ref. [21]). Given the considerable success of these phenomenological studies, one expects that the microscopi-

*jenni.kotila@yale.edu

†Present address: Institut für Kernphysik, Universität zu Köln, Zülpicher Straße 77, D-50937 Köln, Germany; nomura@ikp.uni-koeln.de

cally formulated IBM could also have the potential ability to reproduce the QPT. In this respect, it should be quite interesting to compare the capability to reproduce the first-order QPT between the phenomenological and the microscopic IBM-2 frameworks in a quantitative way.

In this article, we perform both the phenomenological and the microscopic IBM-2 calculations in a series of even-even rare-earth gadolinium and dysprosium isotopes, and compare in detail the two descriptions. Note that by phenomenological calculation we refer to the usual fitting procedure based on the experimental data, and that by microscopical calculation we refer the above-mentioned mean-field-based procedure. We first discuss the energy surfaces for quadrupole deformation, the derived IBM-2 parameters from both approaches, and compare the level energies, $B(\mathrm{E2})$ values, quadrupole moments, and two-neutron separation energies in the isotopes $^{148\text{-}160}$Gd and $^{150\text{-}162}$Dy between the two approaches. The calculations are found to be in qualitative agreement, while quantitative differences occur especially in the transitional region.

The paper is organized as follows: A brief review of the theoretical procedures is given in Sec. II, followed by the spectroscopic observables resulting from the procedures, and the discussion about the results are presented in Sec. III. Conclusion and outlook for possible future studies are given in Sec. IV.

II. THEORETICAL PROCEDURES

A. Choice of Hamiltonian

The IBM in its original version comprises the monopole ($L = 0^+$) s and the quadrupole ($L = 2^+$) d bosons, which represent the collective pairs of valence nucleons. In the present work, we employ the proton-neutron interacting boson model (IBM-2) to describe the quadrupole collective dynamics and quantum phase transitions between these dynamics. The IBM-2 includes the proton (neutron) s_π (s_ν) bosons and the d_π (d_ν) bosons. Since the number of valence protons (neutrons) is fixed for a nucleus, the number of proton (neutron) bosons, denoted as N_π (N_ν), equals half the number of valence protons (neutrons). Eigenstates of quadrupole collective states of interest are generated by the diagonalization of the boson Hamiltonian composed of the basic interactions.

In the present work, the ^{132}Sn doubly-magic nucleus is taken as a boson vacuum for the considered $^{148\text{-}160}$Gd and $^{150\text{-}162}$Dy nuclei. Thus, the neutron boson number N_ν varies from 1 to 7 for both Gd and Dy, corresponding to the $N = 84$–96 nuclei, respectively, while the proton boson number N_π is fixed: $N_\pi = 7$ and 8 for Gd and Dy isotopes, respectively.

We first consider the following Hamiltonian, which is often used in the literature and which is general enough for the phenomenological studies:

$$\hat{H} = \epsilon(\hat{n}_{d_\pi} + \hat{n}_{d_\nu}) - \kappa\,\hat{Q}_\pi^{\chi_\pi}\cdot\hat{Q}_\nu^{\chi_\nu} + \alpha\hat{L}\cdot\hat{L} + \lambda\hat{M}_{\pi\nu} + \frac{1}{2}\sum_\rho\sum_{L=0,2} C_L^\rho[d_\rho^\dagger d_\rho^\dagger]^{(L)}\cdot[\tilde{d}_\rho\tilde{d}_\rho]^{(L)}, \quad (1)$$

where $\hat{n}_{d_\rho} = d_\rho^\dagger\cdot\tilde{d}_\rho$ and $\hat{Q}_\rho^{\chi_\rho} = s_\rho^\dagger\tilde{d}_\rho + d_\rho^\dagger\tilde{s}_\rho + \chi_\rho[d_\rho^\dagger\tilde{d}_\rho]^{(2)}$ represent the d-boson number operator and quadrupole operator for the proton ($\rho = \pi$) and neutron ($\rho = \nu$), respectively. The parameter χ_ρ, which appears in the quadrupole operator, determines the type of the deformation, i.e., the softness in γ degrees of freedom, depending on its sign as well as magnitude. The third term on the right-hand side (RHS) of Eq. (1), $\alpha\hat{L}\cdot\hat{L}$ (denoted the LL term, hereafter), stands for the rotational kinetic-like term, and $\hat{L}$ ($= \hat{L}_\pi + \hat{L}_\nu$) is the boson total angular momentum operator with $\hat{L}_\rho = \sqrt{10}[d_\rho^\dagger\tilde{d}_\rho]^{(1)}$. The fourth term on the RHS of Eq. (1) represents the so-called Majorana term, with its strength λ, given as

$$\hat{M}_{\pi\nu} = -2\sum_{k=1,3}[d_\pi^\dagger d_\nu^\dagger]^{(k)}\cdot[\tilde{d}_\pi\tilde{d}_\nu]^{(k)} + [d_\pi^\dagger s_\nu^\dagger - s_\pi^\dagger d_\nu^\dagger]^{(2)}\cdot[\tilde{d}_\pi\tilde{s}_\nu - \tilde{s}_\pi\tilde{d}_\nu]^{(2)}. \quad (2)$$

The Majorana term is relevant to the proton-neutron mixed symmetry, and has been considered, e.g., in the context of the isovector collective motion of valence shells. Since extensive assessment of the Majorana interaction, including its physical origin, remains to be done, we do not try to touch on this issue here. Also there are several different notations for the Majorana parameters, and we take the one used by Caprio and Iachello [22]. The last term on the RHS of Eq. (1) corresponds to the interaction between like bosons, consisting of respective $L = 0$ and 2 components.

The IBM has its geometrical feature through the coherent-state formalism [23]. The coherent state, denoted by $|\Phi\rangle$, represents the intrinsic state of the boson system and is given as

$$|\Phi\rangle = \prod_{\rho=\pi,\nu}\frac{1}{\sqrt{N_\rho!}}(\lambda_\rho^\dagger)^{N_\rho}|0\rangle \quad (3)$$

with $|0\rangle$ and $\lambda_\rho^\dagger$ being respectively the boson vacuum (inert core) and

$$\lambda_\rho^\dagger = \frac{1}{\sqrt{1+\sum_{\mu=-2}^{2}a_{\rho\mu}^2}}\left(s_\rho^\dagger + \sum_{\mu=-2}^{2}a_{\rho\mu}d_{\rho\mu}^\dagger\right), \quad (4)$$

where $a_{\rho\mu}$ are amplitudes, which are given as $a_{\rho 0} = \beta_\rho\cos\gamma_\rho$, $a_{\rho\pm1} = 0$, and $a_{\rho\pm2} = \frac{1}{\sqrt{2}}\beta_\rho\sin\gamma_\rho$. β_ρ and γ_ρ represent the axially symmetric deformation and the triaxiality for protons and neutrons, respectively. The boson energy surface $E(\beta,\gamma)$ is calculated as an expectation value of the Hamiltonian (1) in terms of the coherent state $|\Phi\rangle$.

A set of the parameters for the IBM-2 Hamiltonian in Eq. (1) is determined for individual nuclei through two types of procedures: the usual fitting procedure starting at the basic experimental data available, and the recently proposed procedure [18], which is based on the mapping of the deformation energy surface [18,19].

In the former approach, all interaction strengths in Eq. (1) are treated as free parameters, which have been determined by the straightforward fit to the experimental data for spectroscopic properties of low-lying states, e.g., the 2_1^+ and 4_1^+ excitation energy and the $B(\mathrm{E2}; 2_1^+ \to 0_1^+)$ value. The parameters ϵ, κ, χ_ν, and α change with N, while common values are used for Gd and Dy isotopic chains. The other parameters are kept constant.

For the latter approach of Ref. [18], however, only those parts of the Hamiltonian (1) up to the third terms are of relevance. The strength parameters for the fourth and the fifth terms on the RHS of Eq. (1) are taken to be zero, as indeed these terms are of little importance in determining the global pattern of the energy surface. This may sound like an oversimplification, but still holds the essential properties of encompassing the dynamics of quantum shape phase transitions in nuclei and illuminating the basic phase structure of a finite nucleus.

We start with the constrained self-consistent Hartree-Fock plus BCS (HF + BCS) calculation using a Skyrme energy density functional (EDF) [24] and obtain the deformation energy surface with quadrupole degrees of freedom, which correspond to the geometrical deformation parameters β and γ [5]. The Skyrme SkM* functional [25] is used throughout, while the following results are not affected much by the particular choice nor the details of the EDFs. Each point on the constrained Skyrme energy surface is mapped onto the corresponding point on the boson energy surface, $E(\beta, \gamma)$. In mapping such an energy surface, we assume that $\beta_\pi = \beta_\nu \equiv \beta_B$ and $\gamma_\pi = \gamma_\nu \equiv \gamma_B$. Here, the variable β_B corresponds to the geometrical β through the proportionality relation $\beta_B = C_\beta \beta$, where C_β is the coefficient irrelevant to the spectroscopic quantities and is determined for an individual nucleus by adjusting the boson β value giving the energy minimum to the fermion one [18]. The C_β value here is typically within the range between 3 and 5, and changes gradually as a function of boson number. γ variables are identical to each other between fermion and boson systems, $\gamma_B = \gamma$. By the mapping of the energy surfaces, the parameters ϵ, κ, χ_π, χ_ν, and the scale factor C_β are determined.

The LL term plays an important role in reproducing the level energies of yrast states for the strongly deformed axially symmetric nuclei like those considered here [20]. To incorporate the LL term, one should go beyond the energy-surface analysis. In Ref. [20], the LL term was determined so that the rotational property, i.e., the rotational cranking, of the nucleon system is reproduced by the boson system. We determined the LL coefficient α by following the procedure of Ref. [20] and, since the LL term does not change the topology of the energy surface,[1] other parameter values ($\epsilon, \kappa, \chi_\pi$, and χ_ν) were kept the same as those determined by the energy-surface analysis.

B. Energy landscape

Figures 1 and 2 show the self-consistent mean-field (left column in each figure), the mapped (middle column), and the phenomenological (right column) IBM-2 energy surfaces for the discussed $^{148-160}$Gd and $^{150-162}$Dy nuclei, respectively. The change in the absolute minimum of the energy surfaces with the neutron number indicates the underlying phase transition as expected.

We first discuss the self-consistent and the mapped IBM-2 energy surfaces. Generally speaking, the mapping from the mean-field to the IBM systems appears to be done reasonably well; namely, the location of the absolute minimum and the curvatures along the β and γ directions of the latter are quite similar to those of former. Nevertheless the mapped IBM-2 energy surfaces are a bit flatter in both β and γ directions for the higher-energy region ($\sim$3 MeV) than the original, self-consistent ones. This is perhaps the consequence of the difference in the size and/or the type of model space between self-consistent mean-field and IBM systems: the former considers all nucleon degrees of freedom, while the latter only valence nucleons.

For both Gd and Dy isotopes, the minimum is located in the vicinity of the origin $\beta = 0$ for $N = 84$ and 86, being close to the vibrational limit; it departs for the prolate side as a function of the neutron number, and reaches around $\beta \approx 0.35$, being at the rotational or SU(3) limit. While qualitatively quite similar systematics is observed for both isotopic chains, the quadrupole correlation is much more pronounced for Dy isotopes. Namely, the energy valley for the Dy isotopes looks generally steeper than that for the Gd. For instance, the deformation energy, that is, the difference in energy between spherical configuration $\beta = 0$ and the minimum point of the boson energy surface, is 9.133 MeV for the ^{160}Dy nucleus, while it is 8.882 for ^{158}Gd. Actually, the Dy isotopes have one more active proton boson that contributes to the deformation than the Gd isotopes.

In the context of the QPT, the drastic change in the topology of the energy surface is expected to occur from $N = 86$ or 88 to 90. Nevertheless, it is rather hard to discern a clear position of the transition point either by the present self-consistent constrained energy surface with the Skyrme EDF or by the mapped IBM-2 energy surface. The change in the topology of the energy landscape in these cases is too gradual to identify the evidence for the critical point X(5) [26]. This is partly because the energy surface is not connected to the spectroscopic observables that can be compared with the available data. Moreover, for those nuclei with $N \approx 88, 90$, which are located in between the two limiting cases, a considerable amount of quantal correlation effect should have been taken into account in the microscopic calculation.

In that sense it is quite useful to compare such an EDF-based energy surface with the one for the phenomenologically determined Hamiltonian, which should reflect the trend expected from the experimental data. The phenomenological energy surfaces are shown in the right columns of Figs. 1 and 2. To make a direct comparison with the microscopic as well as the mapped energy surfaces, the phenomenological boson energy surfaces are drawn in terms of the usual geometrical deformation variables β and γ. The scale factor C_β is introduced here for the β variable as well, which is determined so that the experimental β_2 values for $N = 94$ nuclei [27] are reproduced. Since there is no available experimental β_2 values for lighter ($N \leqslant 86$) nuclei, the fixed values C_β =2.827 and 2.757 are used for simplicity for Gd and Dy isotopes, respectively. We note that, as no connection is made between

[1]The expectation value of the LL term has the same form as that of the d-boson number operator, except for the coefficient 6α. To keep the mapped energy surface, the parameter ϵ is shifted by $\Delta\epsilon = 6\alpha$ when diagonalizing the Hamiltonian [20].

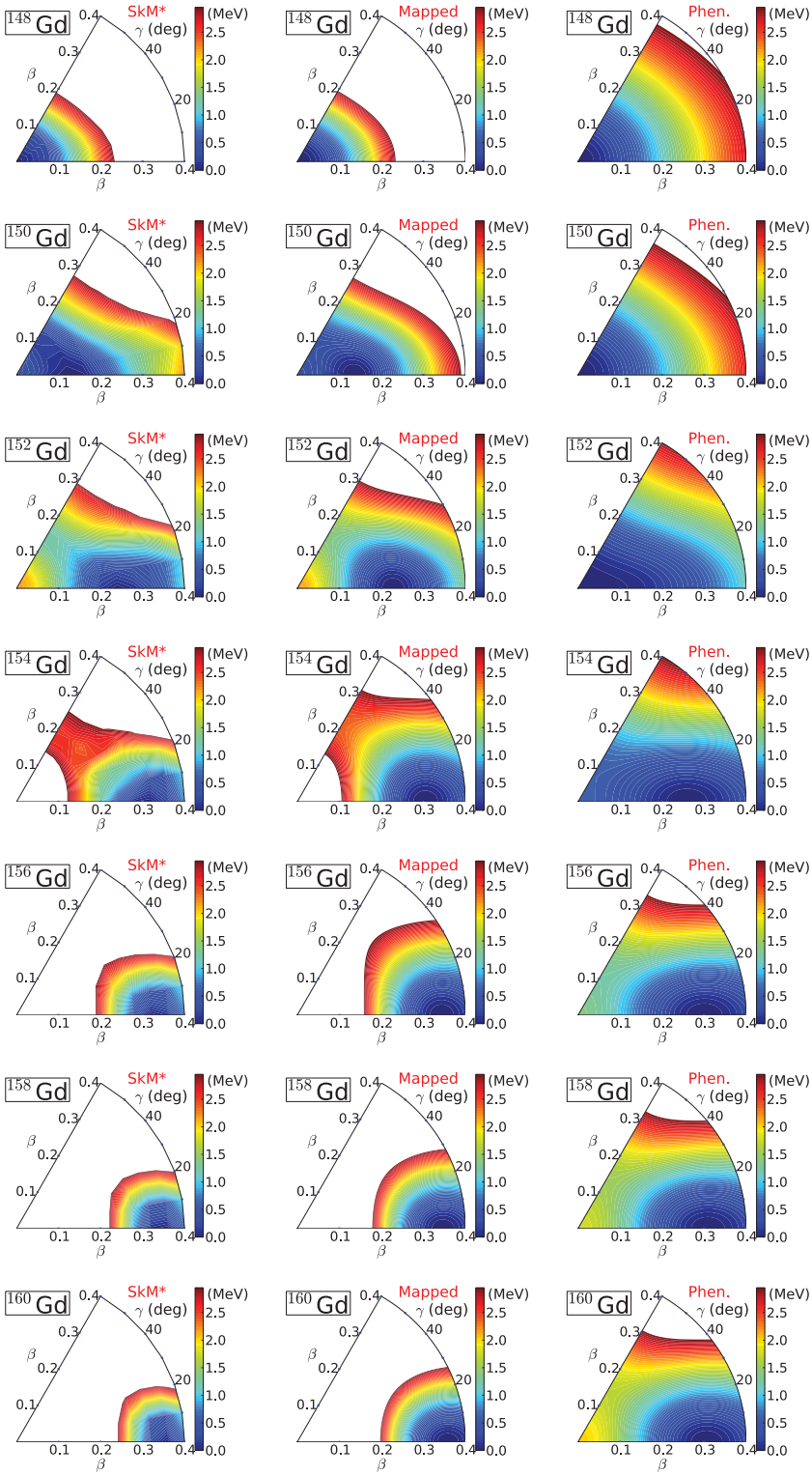

FIG. 1. (Color online) Energy surfaces of the $^{148-160}$Gd nuclei, obtained from (left) the Skyrme HF + BCS calculation, and from the mapped (middle) and the phenomenological (right) IBM-2 Hamiltonians.

microscopic self-consistent and phenomenological energy surfaces, one should not use the same C_β values as those in the mapped energy surfaces for the phenomenological ones. The proton and the neutron β (γ) variables are assumed to be identical to each other, similarly to the mapped IBM-2 surface.

It is clear from Figs. 1 and 2 that the phenomenological energy surfaces differ significantly from the microscopic (both the self-consistent mean-field and the mapped) energy surfaces in the following respects: (i) The former is generally much flatter in the topology along both β and γ directions than the latter. A notable difference is seen for the $N = 88$ nuclei: both the self-consistent and the mapped energy surfaces suggest an already well deformed configuration, while the phenomenological ones have minima in the vicinity of the

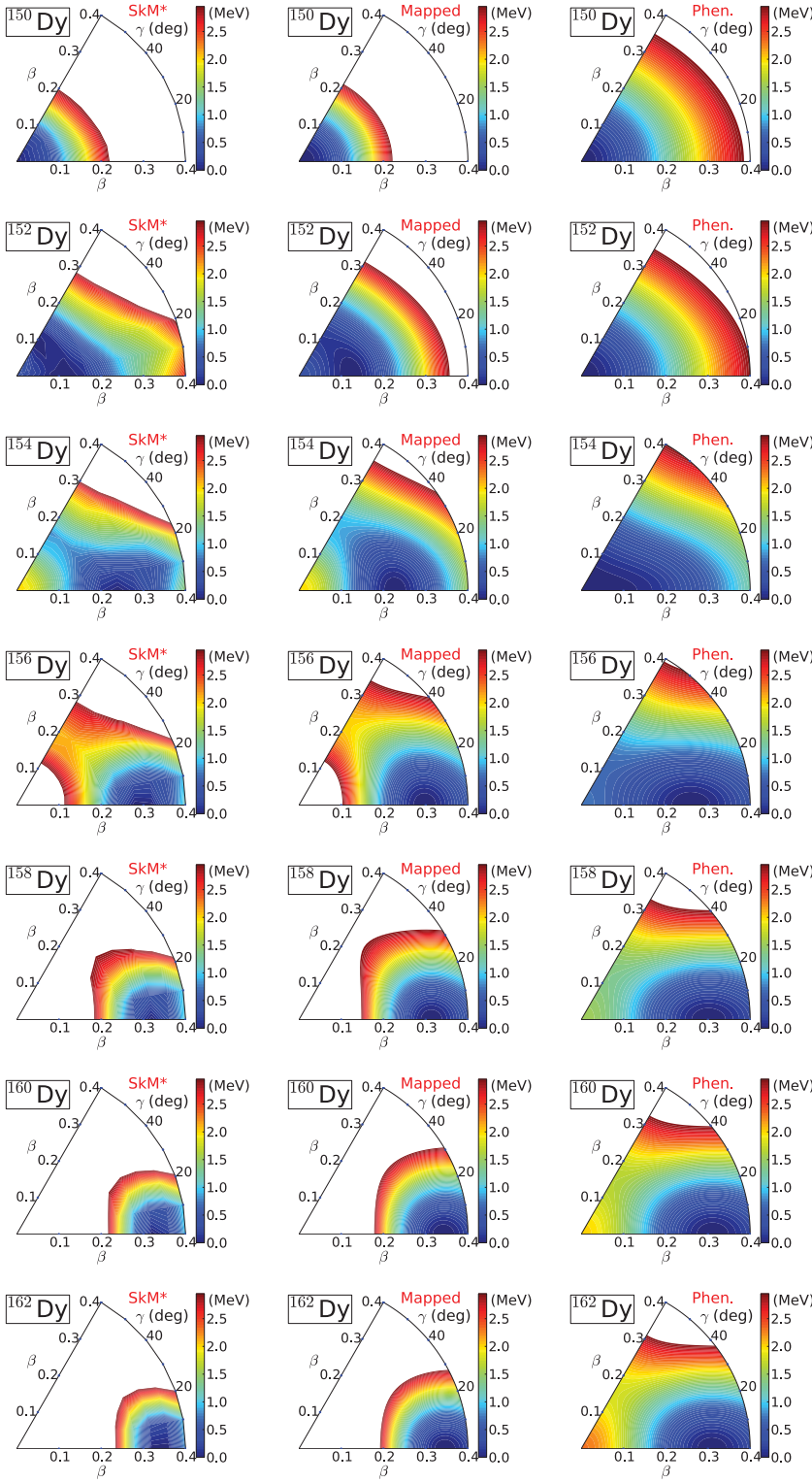

FIG. 2. (Color online) Same as Fig. 1, but for the $^{150-162}$Dy nuclei.

origin. (ii) No sudden change in the minimum point along the β direction is seen in the self-consistent or mapped energy surfaces. In the microscopic energy surface, the minimum shifts rather moderately from $N = 84$ to 88. There is, however, a jump of the minimum point from $N = 88$ to 90 for phenomenological energy surfaces, which is more consistent with the experimental tendency of the level energies. As one will see, these differences between the phenomenological and the microscopic energy surfaces are reflected in the resultant spectroscopy.

C. IBM parameters

Evolution of the relevant parameters of the boson Hamiltonian in Eq. (1) are shown in Figs. 3 and 4, obtained through

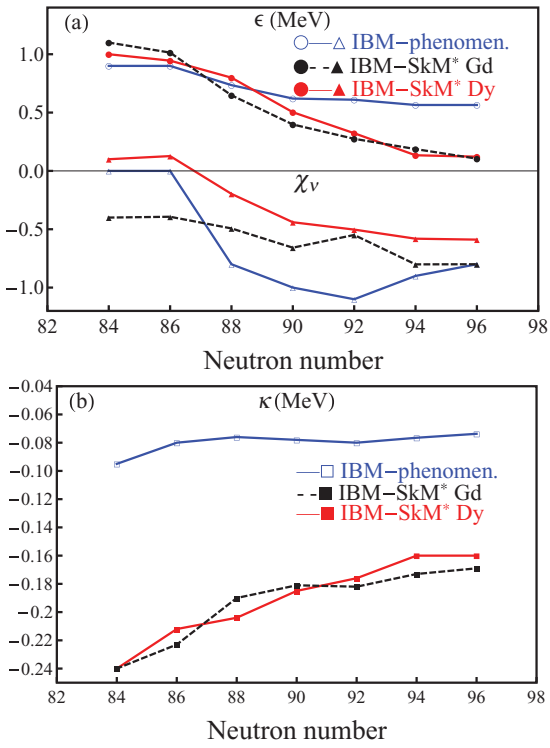

FIG. 3. (Color online) The IBM-2 parameters (a) ϵ (MeV) and χ_ν, and (b) κ (MeV) for the considered nuclei obtained from the two approaches: the usual phenomenological fitting method (denoted IBM-phenomenology) and the energy-surface-based mapping procedure, denoted IBM-SkM*.

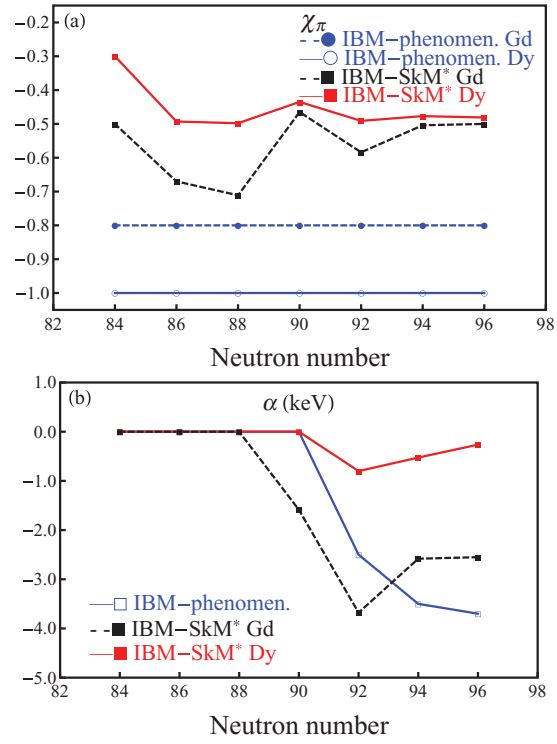

FIG. 4. (Color online) The derived IBM-2 parameters (a) χ_π and (b) α (keV) for Gd and Dy isotopes. In the IBM-phenomenology calculation χ_π is fixed: $\chi_\pi = -1.0$ and $\chi_\pi = -0.8$ for Gd and Dy isotopes, respectively.

the usual phenomenological fitting calculations, denoted IBM-phenomenology, and the mean-field-based method of Ref. [18] (denoted IBM-SkM*). For the sake of simplicity, the Hamiltonian parameters other than ϵ, κ, χ_ν, and α are fixed in the former approach: For Gd (Dy) isotopes, $\chi_\pi = -1.0\,(-0.8)$, $C_0^\pi = -0.20\ (-0.05)$ MeV, and $C_2^\pi = -0.10\ (-0.15)$ MeV, while $C_0^\nu = C_2^\nu = 0$ MeV and $\lambda = 0.04$ MeV for both isotopic chains. In the latter approach, $C_L^\rho = \lambda = 0$ MeV, as already mentioned.

In Fig. 3(a), the parameter ϵ exhibits roughly the same behavior for both calculations up to the critical-point nucleus $N \approx 90$. For heavier isotopes, the ϵ value decreases gradually in the IBM-phenomenology calculation, but more rapidly in the IBM-SkM* one.

Notable quantitative differences between the two calculations are observed in some of the derived IBM parameters. For instance, in Fig. 3(b), the magnitude of the κ parameter in the IBM-SkM* calculation is generally much larger than the one in the IBM-phenomenology calculation. This is not only because the IBM-2 Hamiltonian used in the IBM-SkM* approach is too simple, but also because of the peculiar topology of the self-consistent mean-field energy surface with the Skyrme EDF, which is rather different from what is expected from the phenomenological result. Such a quantitative difference of the κ parameter between the EDF-based and the phenomenological calculations is a decisive factor that gives rise to deviation of the level energies of the non-yrast states.

Going back to Fig. 3(a), the trend of the χ_ν parameter is similar for both types of calculations, even though the IBM-SkM* calculation does not show such a rapid drop in the values as the IBM-phenomenology calculation. This is not surprising, given the trends of the energy surfaces in Figs. 1 and 2.

The proton χ_π parameter is taken as a constant for each isotopic chain in the phenomenological calculation. In the IBM-SkM* calculation, the values vary between -0.5 and -0.711 in the Gd isotopes and between -0.3 and -0.491 in the Dy isotopes but do not change too much, as shown in Fig. 4(a). The situation is thus reversed as in the case of parameter κ, and the magnitude of the χ_π parameter in the IBM-phenomenology calculation is generally larger than the one in the IBM-SkM* calculation.

The magnitude of the sum $\chi_\pi + \chi_\nu$ (with negative sign) increases with neutron number N, reflecting the onset of the larger quadrupole deformation with N. This feature is also consistent with the mapped IBM-2 energy surface, which becomes more rigid at $\gamma = 0^\circ$ with N.

The derived LL strength is shown in Fig. 4(b). The LL term is relevant to rotational nuclei with large quadrupole deformation, and is taken into account for $N \geqslant 90$ and 92 Gd and Dy nuclei, respectively. Actually, those deformed Gd and Dy isotopes have $R_{4/2} \gtrsim 3.2$, for which the rotor formula is quite a good approximation. Concerning the lighter nuclei whose $R_{4/2}$ ratios are well below 3.2, the LL parameter α is taken to be zero as, in that case, it has only a minor impact on the rotational moment of inertia [20]. Indeed, the calculated yrast spectra for the nuclei in latter category are already in good

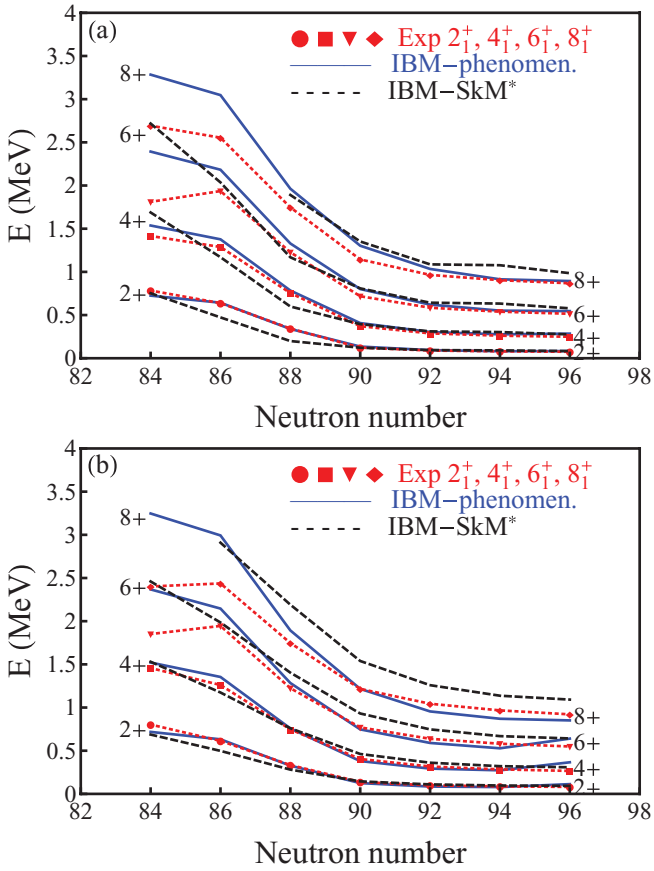

FIG. 5. (Color online) Evolution of the low-lying ground-state band energies for (a) $^{148–160}$Gd and (b) $^{150–162}$Dy isotopes.

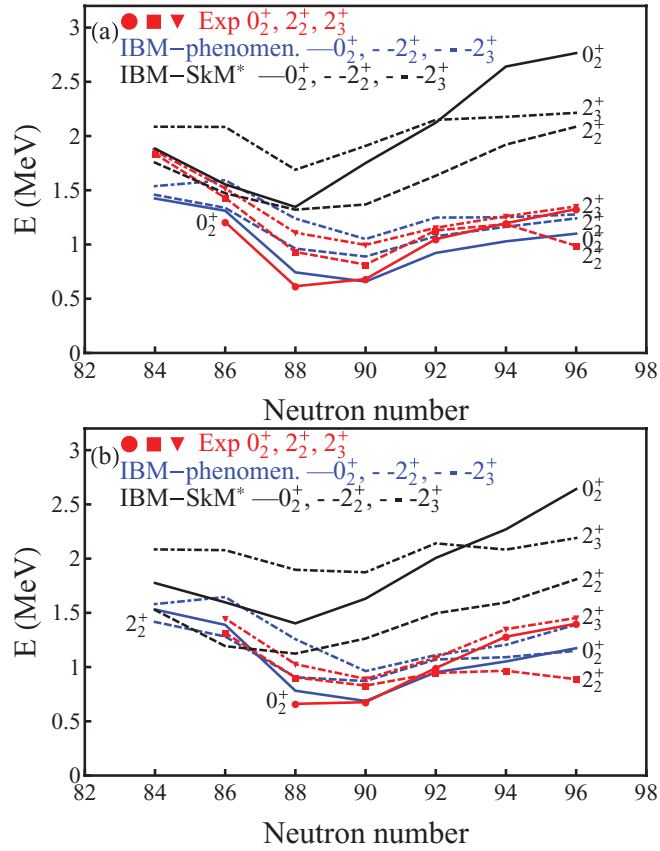

FIG. 6. (Color online) Evolution of the excited states 0_2^+, 2_2^+, and 2_3^+ for (a) $^{148–160}$Gd and (b) $^{150–162}$Dy isotopes.

agreement with the experimental data, as one will see later in Figs. 5(a) and 5(b). In general for the IBM-SkM* calculation, notably larger magnitudes are needed for gadolinium isotopes than dysprosium isotopes, the largest being for ^{156}Gd. In the case of the phenomenological calculation, the same value of α is taken for both isotopic chains, and a larger magnitude of parameter α is taken as N increases.

III. RESULTS AND DISCUSSION

Having the parameters, including those shown in Figs. 3 and 4, one can calculate the excitation spectra, the reduced E2 transition probabilities B(E2), quadrupole moments, and the two-neutron separation energies. The computer program NPBOS [28] is used to diagonalize the Hamiltonian of Eq. (1). Results of the calculations are shown in Figs. 5–13.

A. Level energies

Figures 5(a) and 5(b) show the evolution of the ground-state band energies in the considered gadolinium and dysprosium nuclei, respectively.

A quick look reveals that both calculated spectra become more compressed with increasing N, following the experimental trend [27]. Around $N = 86$, the spectra look like those of spherical vibrators [or U(5) limit]. As the number of bosons (i.e., the valence neutrons) increases, levels come down consistently with the experimental trends. Around $N = 90$ there seems to be evidence for the X(5) critical-point symmetry in the experimental spectra. Both isotopic chains also show close-lying set of states in experimental spectra for $N = 84$, which cannot be reproduced by theoretical calculations due to the limited degrees of freedom for the IBM model space consisting of s and d bosons. These states are also of two-quasiparticle character rather than collective states. For $N = 86$ the situation is different and both theoretical calculations give reasonable agreement with experimental data. Rotational features are found for both isotopic chains as $N \geqslant 90$ in both theoretical spectra and experimental spectrum.

The evolution of the excited states for the non-yrast bands, namely 0_2^+, 2_2^+, and 2_3^+, is shown in Figs. 6(a) and 6(b). In the phenomenology, one is able to reproduce fairly well the drop in excited energies observed in experimental spectra. The lowest-level energies are seen around $N = 88–90$, corresponding to the X(5) critical point, beyond which 0_2^+, 2_2^+, and 2_3^+ states go up in both experiment and calculation. The IBM-2 phenomenology calculation is able to reproduce the trend of these sideband energies at the quantitative level, whereas the mapped IBM-2 predicts levels much higher than the experimental and the phenomenological values, although

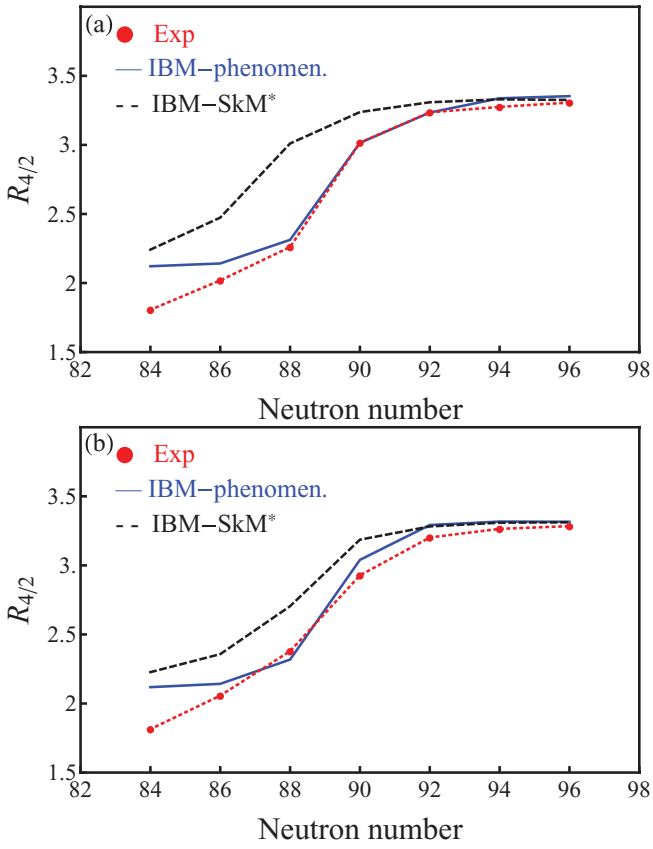

FIG. 7. (Color online) Evolution of the ratio $R_{4/2} = E(4_1^+)/E(2_1^+)$ for (a) $^{148–160}$Gd and (b) $^{150–162}$Dy isotopes.

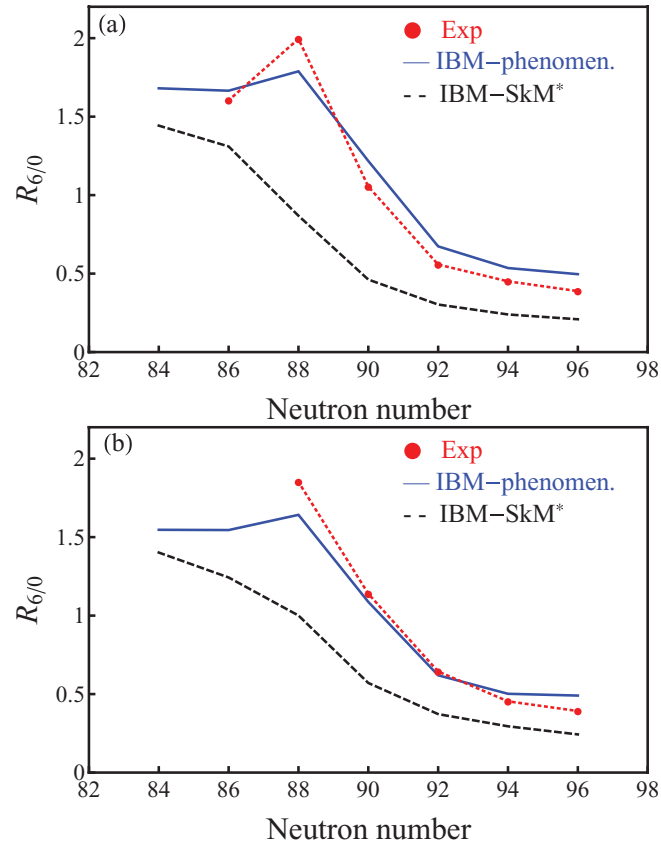

FIG. 8. (Color online) Evolution of the ratio $R_{6/0} = E(6_1^+)/E(0_2^+)$ in (a) $^{148–160}$Gd and (b) $^{150–162}$Dy isotopes.

the overall pattern is rather well reproduced. A direct reason for this is the too-large value of the parameter κ in the EDF-based approach compared to the one in the phenomenological calculation. Experimental spectra also show a low-lying 2_2^+ state for isotone $N = 96$, which is not well described by either calculation.

Next we have a closer look at the signatures of the shape phase transition. To such an end, we discuss the behavior of the ratio $R_{4/2} = E_x(4_1^+)/E_x(2_1^+)$ shown in Fig. 7. For both isotopic chains, one observes in their experimental data the systematic trend of the evolution of the ratio $R_{4/2}$ from $R_{4/2} \simeq 2$, corresponding to the spherical vibrational limit, to $R_{4/2} \simeq 3.3$, the axially deformed rotor limit. This behavior reveals the occurrence of the shape phase transition in the considered isotopic chains. We obtain a reasonably good agreement between the experimental data and the IBM-phenomenological results in the vibrational and rotational limits as well as in the transitional nuclei, including the nearly critical-point ($R_{4/2} = 2.91$) [26] nuclei at $N = 90$, while some deviations are observed in IBM-SkM* calculation in the transitional $N = 86$–90 nuclei as well as in the vibrational limit. The IBM-phenomenology calculation produces a rapid transition at $N = 90$, similar to the data, while the EDF-based approach does not indicate a clear transition point, as we pointed out before. A similar kind of argument seems to hold in the same rare-earth region in some other major microscopic frameworks, such as the projected configuration-mixing calculation [11]. One also notices that the experimental $R_{4/2}$ ratio for nuclei with neutron number $N = 84$ is smaller than 2, suggesting either that these nuclei may be no longer collective or that the situation is out of the model space of *sd* IBM.

An additional stringent test for the first-order QPT is the ratio $R_{6/0} = E_x(6_1^+)/E_x(0_2^+)$, which is characterized by its anomalous kink at around the transitional nuclei [29]. Figures 8(a) and 8(b) display the ratio for the considered $^{148–160}$Gd and $^{150–162}$Dy isotopes, respectively. For the $N = 84$ and 86 nuclei, which are close to the harmonic vibrator limit, $R_{6/0} = 1.5$, according to Fig. 8. As N increases, the ratio $R_{6/0}$ goes down and in the rotor limit it is well below unity. At the critical point this ratio is close to unity ($R_{6/0} = 0.96$). Both isotopic chains show a small increase in this ratio when moving from $N = 86$ to $N = 88$ and then a rapid drop to $N = 90$. The kink at $N = 88$ in the experimental data is explained by the rapid decrease of the 0_2^+ excitation energy. This behavior is well reproduced by the IBM-phenomenology calculation, whereas the IBM-SkM* predicts a much smoother evolution. Such a discrepancy between the two calculations occurs because of the behavior of the 0_2^+ excitation energy as shown in Figs. 6(a) and 6(b). In the IBM-SkM* calculation the 0_2^+ excitation energy exhibits also the kink around $N = 88$ or 90, similar to the IBM phenomenology, but it is more gradual and is predicted to be too large.

B. B(E2) values

Once the wave functions of the excited states are generated by the diagonalization of the Hamiltonian in Eq. (1), one can calculate the electromagnetic transition probabilities between the states of interest. The reduced E2 transition probability [B(E2) value] for the transition from the state with spin L_i^+ to the state with spin L_f^+ is of primary importance, and is defined as

$$B(\mathrm{E2}; L_i \to L_f) = \frac{1}{2L_i+1}|\langle L_f||\hat{T}^{(\mathrm{E2})}||L_i\rangle|^2, \qquad (5)$$

where $\langle L_f||\hat{T}^{(\mathrm{E2})}||L_i\rangle$ stands for the reduced matrix element of the E2 operator $\hat{T}^{(\mathrm{E2})}$. Here the E2 operator $\hat{T}^{(\mathrm{E2})}$ is given as $\hat{T}^{(\mathrm{E2})} = e_\pi \hat{Q}_\pi^{\chi_\pi} + e_\nu \hat{Q}_\nu^{\chi_\nu}$, where e_ρ stands for the effective charges for proton and neutron bosons. We here take the fixed values of $e_\pi = 0.177$ and $e_\nu = 0.059$ (in eb units) for both the phenomenological and the energy-surface-based approaches. We here note that, for the latter approach, the effective charges should be derived from the fermion calculation. This is, in practice, quite difficult because the treatment of the effect beyond the mean field; i.e., the core polarization, should be taken into account. This is one of our ongoing projects, but here we end up with the same set of effective charges as the one determined in a phenomenological way.

Figure 9 shows the B(E2) values for the E2 transitions between the states of the ground-state band, $B(\mathrm{E2}; L \to L-2)$ with $L \geqslant 2$. These B(E2) values increase as the collectivity becomes enhanced with N. This is most highlighted by the $B(\mathrm{E2}; 2_1^+ \to 0_1^+)$ value for both considered isotopes in Fig. 9, where the sudden change is observed from $N = 88$ to 90. Again, theoretical calculations follow the experimental data quite nicely. The B(E2) values increase as N increases, pointing to phase transition, as already seen from the excitation energies.

It was suggested in Refs. [37,38] that the E2 transition $2_3^+ \to 0_2^+$ can be a very sensitive signature of the shape phase transition. In Ref. [37] the ratio $B(\mathrm{E2}; 2_3^+ \to 0_2^+)/B(\mathrm{E2}; 2_1^+ \to 0_{gs}^+)$ was taken as an additional observable that is very sensitive to the control parameter ζ, which is translated into the ϵ/κ ratio [see Eq. (1)]. We here look at the $B(\mathrm{E2}; 2_3^+ \to 0_2^+)/B(\mathrm{E2}; 2_1^+ \to 0_{gs}^+)$ ratios as a function of the $E_x(2_1^+)$ shown in Fig. 10. The ϵ/κ ratio decreases with the neutron number N. Likewise, the 2_1^+ excitation energy decreases naturally with N and is hence taken as the quantity we look at here, rather than the ϵ/κ ratio, because both the $B(\mathrm{E2}; 2_3^+ \to 0_2^+)/B(\mathrm{E2}; 2_1^+ \to 0_{gs}^+)$ ratio and the energy $E(2_1^+)$ are measurable quantities. As one sees in Figs. 10(a) and 10(b), the ratio $B(\mathrm{E2}; 2_3^+ \to$

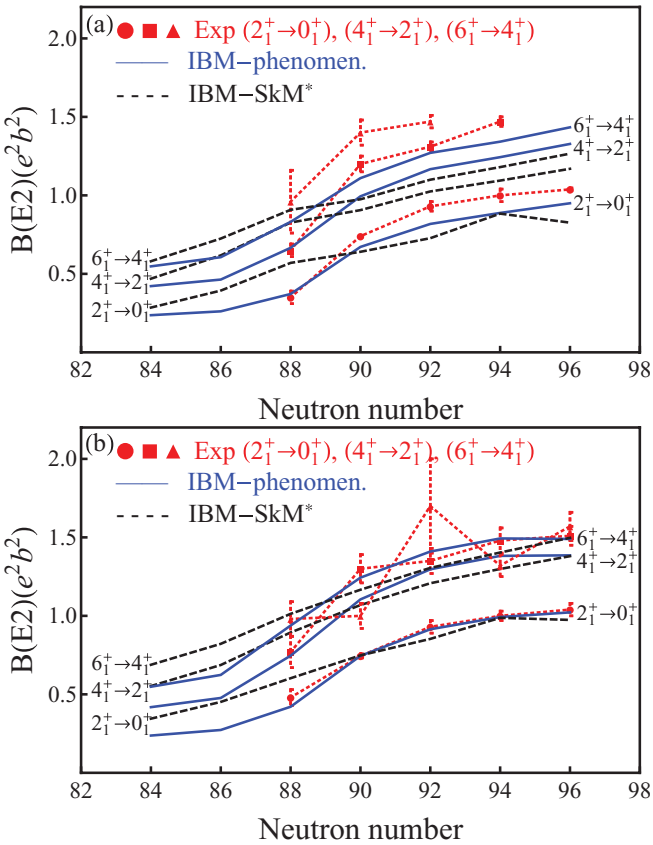

FIG. 9. (Color online) Experimental [30–36] and theoretical B(E2) values (in e^2b^2 units), $B(\mathrm{E2}; 2_1^+ \to 0_{g.s}^+)$, $B(\mathrm{E2}; 4_1^+ \to 2_1^+)$, $B(\mathrm{E2}; 6_1^+ \to 4_1^+)$, and $B(\mathrm{E2}; 8_1^+ \to 6_1^+)$, for (a) $^{148-160}$Gd and (b) $^{150-162}$Dy isotopes.

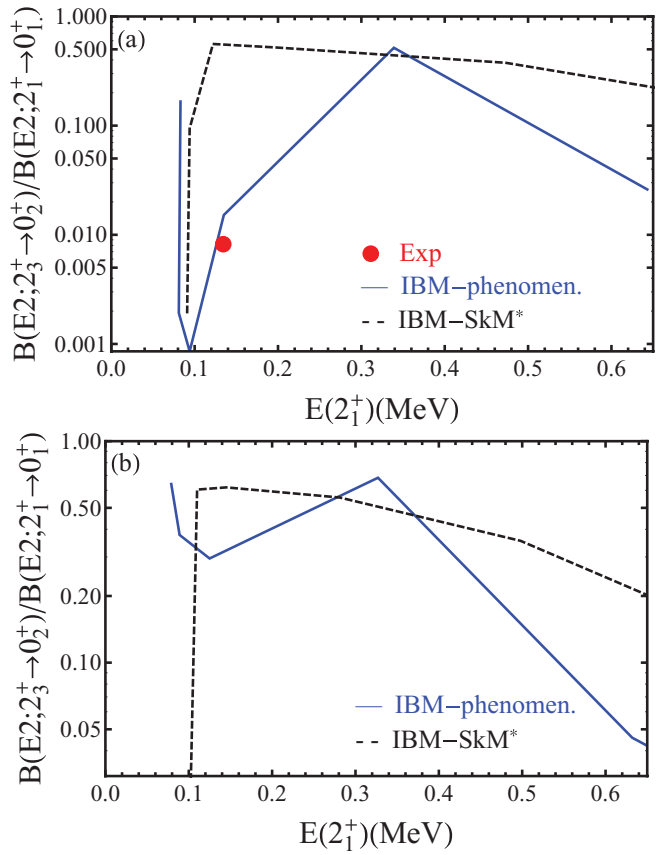

FIG. 10. (Color online) The $B(\mathrm{E2}; 2_3^+ \to 0_2^+)/B(\mathrm{E2}; 2_1^+ \to 0_{gs}^+)$ ratios as a function of the $E_x(2_1^+)$ for (a) $^{148-160}$Gd and (b) $^{150-162}$Dy isotopes. The only experimentally known value is $B(\mathrm{E2}; 2_3^+ \to 0_2^+)/B(\mathrm{E2}; 2_1^+ \to 0_{gs}^+) = 0.0797$ [31], for the ^{154}Gd nucleus. Note that the vertical axis is in logarithmic scale.

$0_2^+)/B(\mathrm{E2};2_1^+ \to 0_{gs}^+)$ vanishes rapidly when approaching the critical-point nucleus.

As one can see in Fig. 10(a), for gadolinium isotopes there is a rapid drop to zero at $N = 88$, which also suggests that there could be coexisting deformed and spherical structures. Actually, this E2 transition is experimentally hard to measure, and the only known value is $B(\mathrm{E2};2_3^+ \to 0_2^+)/B(\mathrm{E2};2_1^+ \to 0_{gs}^+) = 0.0797$ for the ^{154}Gd nucleus. In the case of dysprosium isotopes, there are no available experimental data, and theory does not predict changes as striking as in Gd isotopes.

C. Quadrupole moments

We then study the quadrupole moments. The quadrupole moment Q_L for the state with spin L is defined as

$$Q_L = \sqrt{\frac{16\pi}{5}} \begin{pmatrix} L & 2 & L \\ -L & 0 & L \end{pmatrix} \langle L||\hat{T}^{(\mathrm{E2})}||L\rangle, \qquad (6)$$

where the parentheses () stand for the 3-j symbol (or Clebsch-Gordan coefficient). A good measure of the collective structure would be the quadrupole moment for the 2_1^+ excited state, denoted $Q_{2_1^+}$. Figure 11 shows the calculated and the experimental $Q_{2_1^+}$ values.

Development of the nuclear deformation can be seen from the neutron closed shell at $N = 82$ toward the open-shell nuclei, and also with this quantity a rapid change is seen around $N = 90$. Experimental data is only available for the $N \geqslant 90$ nuclei, where both theoretical predictions are similar to each other and give good agreement with the data. This observation is in conflict when compared to the microscopic calculation of Ref. [39], where a steady increase in magnitude is obtained and the predicted nuclear deformation is always larger than the experimental data.

D. Separation energies S_{2n}

In this section we study the QPT from the perspective of some ground-state properties. Among others, the evolution of the ground state two-neutron separation energies, S_{2n}, as a function of neutron number is very sensitive to the details of nuclear structure [40,41]. This observable is defined as the difference in binding energy between an even-even isotope and the preceding even-even isotope:

$$S_{2n} = E_B(N, Z) - E_B(N-2, Z), \qquad (7)$$

where $E_B(N, Z)$ stands for the binding energy for the nucleus with N and Z. In the IBM-2, the binding energy is nothing but the eigenenergy of the ground state (the 0_1^+ state) plus the

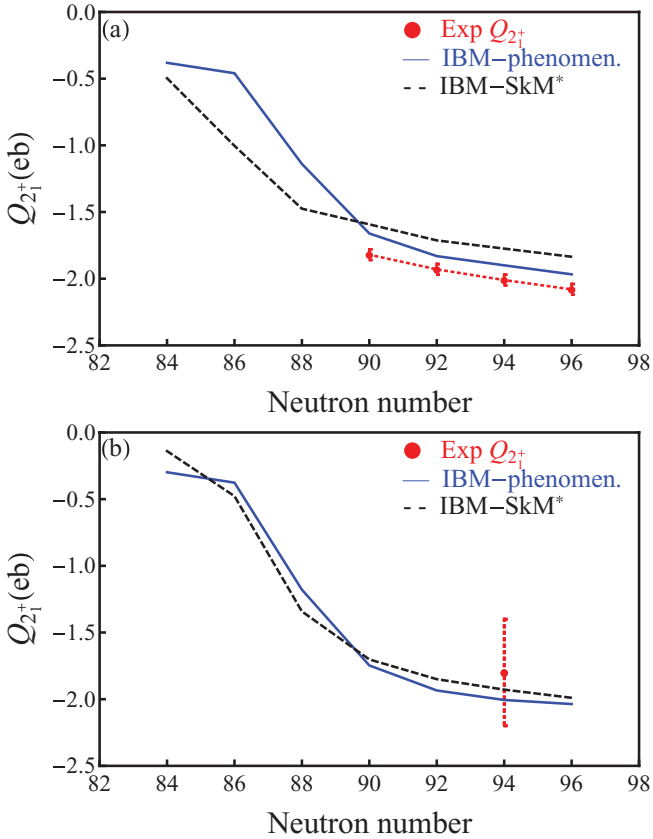

FIG. 11. (Color online) Experimental [30–33] and theoretical quadrupole moments $Q_{2_1^+}$ (in eb units) for (a) $^{148-160}$Gd and for (b) $^{150-162}$Dy isotopes.

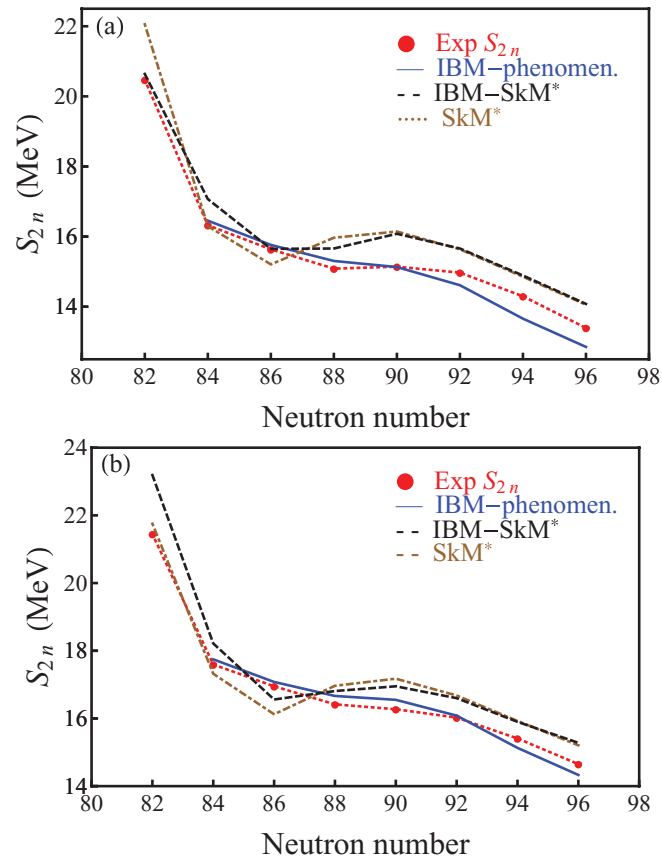

FIG. 12. (Color online) Experimental and theoretical two-neutron separation energies S_{2n} for (a) $^{148-160}$Gd and for (b) $^{150-162}$Dy isotopes.

global term that linearly depends on the number of bosons [16]. The coefficients of the global term are determined from the fitting to the experimental binding energy in the IBM-phenomenology approach and from the self-consistent mean-field calculation in the IBM-SkM*. The way to obtain the binding energy in the latter approach is explained in detail in Ref. [19].

As a function of neutron number, S_{2n} shows well known regularities: for any fixed number of protons, S_{2n} decreases smoothly as the number of neutron increases. A detailed discussion of the properties of S_{2n} can be found, e.g., from Ref. [42].

As has been often noted so far, nuclei with $N \approx 90$ are known [43–47] to be examples of the X(5) critical point, and this special behavior can be seen in the evolution of S_{2n} with N as shown in Fig. 12, where the two-neutron separation energies show a pronounced plateau. In Ref. [48] the behavior of samarium isotopes was studied by means of IBM-1. A similar analysis is performed here also. The separation energies should in general behave linearly. This is exactly the case when looking at the experimental, as well as theoretical, two-neutron separation energies for Gd and Dy isotopes with $N \leqslant 88$ and $N \geqslant 92$. In the transitional region between the U(5) and the SU(3) limits, however, one observes a plateau, which is indeed seen in the experimental evolution of S_{2n}. This change is reproduced reasonably well by the phenomenological calculation, even though it is not as sharp as in the experimental data, and by the microscopic IBM-2 calculation and the mean-field solution (denoted as SkM*) as well, shown also in Fig. 12. The difference of the S_{2n} between IBM-SkM* and SkM* comes from the quantum-mechanical correlation effect taken into account by the diagonalization of the boson Hamiltonian in the laboratory frame, which is not included in the latter. Although the difference is very small, the inclusion of the correlation effect improves the agreement between the IBM-SkM* and the experimental S_{2n} a little for the nuclei in the vicinity of the neutron closed shell $N = 82$. This is a rather sound result and is also consistent with what is concluded in our previous work on Sm isotopes [19].

As the evolution of the two-neutron separation energies confirms, according to our calculations the $N = 90$ isotones ^{154}Gd and ^{156}Dy could be considered as candidates for X(5) nuclei.

E. X(5) critical-point nuclei

As all the observables discussed above suggest, the $N = 90$ isotones ^{154}Gd and ^{156}Dy seem to be good candidates for X(5) nuclei. It is interesting to look at the level spectra of these nuclei in more detail and compare them with the spectrum of X(5) symmetry [26]. This is done in Fig. 13. In terms of the X(5) symmetry the figure shows the $s = 1, 2$ sequences, with s denoting a quantum number in the X(5) model.. Comparison between experimentally observed spectra and an analytic description of critical-point X(5) nuclei is extremely close for ^{154}Gd, a bit further for ^{156}Dy, and in agreement with Ref. [43] in the case of ^{152}Sm. Comparison with the $s = 1$ sequence shows

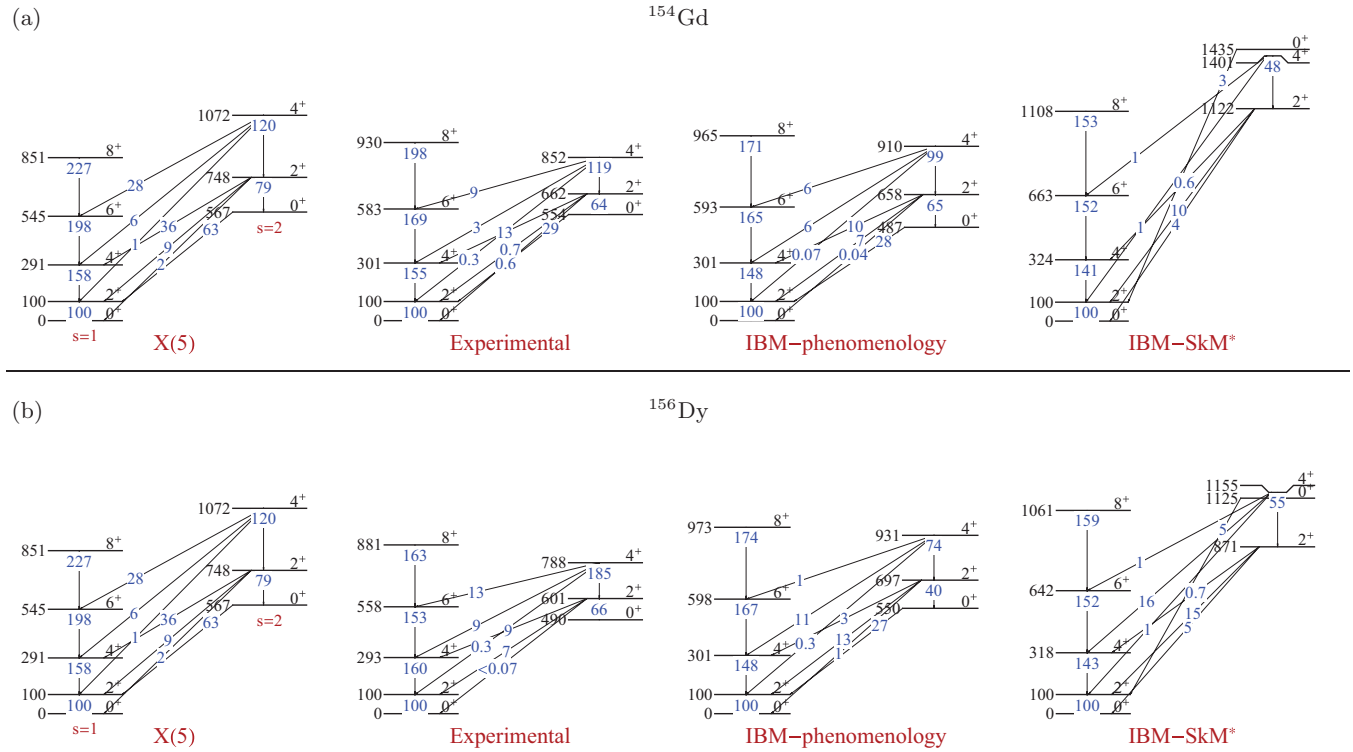

FIG. 13. (Color online) Spectrum of X(5) symmetry compared with experimental and theoretical spectra for (a) ^{154}Gd and for (b) ^{156}Dy isotopes. Energies are in units of the first excited state, $E_x(2_1^+) = 100$, and B(E2) values are in units of $B(\mathrm{E2}; 2_1^+ \rightarrow 0_1^+) = 100$.

that the phenomenological IBM-2 calculation overestimates slightly the excitation energies of 6_1^+ and 8_1^+ states, and the corresponding transition strengths are found to be slightly underestimated, whereas for the $s = 2$ sequence both the energies and transition strengths are slightly underestimated. The transitions between the two sequences are also reproduced rather well. A more clear difference is seen when comparing experimental or X(5) symmetry to the microscopical IBM-2 calculation which, compared to the $s = 1$ sequence, shows a pattern that is already a rotor. Compared to the $s = 2$ sequence the energies are too high due to a too-large value of the parameter κ in the EDF-based approach, as already discussed. However, comparison with the transition strengths for the $s = 2$ sequence, as well as for the transitions from $s = 2$ to $s = 1$, are in acceptable agreement with the X(5) symmetry.

When comparing the two $N = 90$ isotones to each other in view of X(5) symmetry, the ^{156}Dy nucleus is found to be of slightly poorer quality than ^{154}Gd, as is also discussed in Refs. [44–46]. In the current study this conclusion is mainly made by comparing the transition probabilities of the first excited band, $s = 2$, and those of the interband transitions between $s = 1$ and $s = 2$.

In the microscopic IBM-2 calculation, neither choosing other sets of parameters nor adding any other interaction terms in the Hamiltonian in Eq. (1) seems to be helpful in reproducing the experimental sideband ($s = 2$) energies. The deviation of the $s = 2$ band originates from either the mapping procedure in its current version or the energy density functional itself. The former possibility may concern the treatment of boson number in the coherent state of Eq. (3), which could be taken to be larger than as it is. Actually, to describe the QPT the boson number in the coherent state is often taken to be sufficiently large, and hence may not necessarily be the same as the one in the usual boson-number counting rule, which assumes the nearest doubly-magic nucleus as the inert core [17]. Such an argument could meet the self-consistent mean-field calculation carried out here, where particle number is still not treated exactly. Mapping the energy surface projected onto a state with any good symmetry may resolve the problem as well. Concerning the latter possibility, the microscopic (both original and mapped) energy surfaces for $N = 90$ isotones in Figs. 1 and 2 are too steep compared to the energy surfaces based on the phenomenologically determined IBM parameters. Certainly, the difference in the topology results in the deviation of the sideband energies, and may be due to the property of the employed EDF itself. A similar conclusion has been extracted in many microscopic EDF-based theories that are found in the literature, using other types of EDFs. This is not too surprising, as a universal EDF has not been found.

IV. CONCLUSIONS

To conclude, spectroscopic calculations have been carried out for the even-even gadolinium and dysprosium isotopes to examine the shape phase transition between the spherical vibrational and the deformed rotational states. Spectroscopic properties, which help identify the shape transition, have been analyzed: the level energies, the B(E2) values, the quadrupole moments for the 2_1^+ excited state, and the two-neutron separation energies. Two types of the IBM-2 calculations have been made to generate these quantities: one is a conventional fitting calculation based on the available experimental data for the excitation energies, while the other is a derivation of the IBM-2 Hamiltonian based on the constrained self-consistent mean-field method with Skyrme functional SkM*.

Comparisons between these two methods and experiments were made, and it was found that both approaches give equally reasonable agreement with the experimental spectroscopic data as far as the yrast states are concerned. In the former approach, experimental spectra, including those of the side-bands, have been reproduced at almost perfect level. The $N \approx 90$ nuclei show also properties suggesting them to be very close to the X(5) critical point of the vibrator-to-axial-rotor shape transition, and the ^{154}Gd might be a nucleus exhibiting coexistence of spherical and deformed phases. In the latter approach, however, while the overall systematic trend of the experimental non-yrast levels such as the bandhead of the β and γ bands, 0_2^+ and 2_2^+, respectively, were traced rather well, the absolute values of these energy levels are much higher than the observed energies. In addition, the evolution of the key observables as functions of neutron number seemed to be more or less smeared out, not exhibiting a clear critical point as is found in the phenomenological approach.

Also, it was suggested in the EDF-based method that the nuclei close to the neutron closed shell $N = 82$, such as $N = 84$ and 86 nuclei, and the transitional nuclei ($N = 88$ and/or 90) as well, seem to be much more deformed than expected from the experimental systematics. Such a feature seems to arise in the microscopic Skyrme EDF calculation already, irrespectively of the choice or the details of the density functionals [19]. A possible reason for this is that the EDF energy surface still may not give a good approximation because, for instance, the particle number is not conserved in the Skyrme EDF calculation. This would severely affect the transitional nuclei, where a sizable amount of quantum fluctuation should be fully taken into account. The problem does not show up in the phenomenological approach as it is not connected to any microscopic picture, but such a phenomenological study is, of course, not consistent with the microscopic calculation. It should be interesting to clarify in the future why the phenomenologically determined IBM-2 Hamiltonian is that different from what is predicted by the microscopic EDF.

Another future work which could be done along the same line would be to identify the first-order QPT in other mass regions. The region with mass $A \approx 100$, that is, the Kr-Sr-Zr-Mo-Ru region, can be a good example for this, as there has been evidence for a transition between spherical and axially deformed ground-state shapes. Since, in such a lighter mass region, not only the collective but also the single-particle degrees of freedom may enter, it is of interest to find out whether or not the simple schematic model of QPTs still holds. The phenomenological aspects of the $A \simeq 100$ region are similar to those of the $A \simeq 150$ region: The onset of deformation appears to be sharp for Sr-Zr but smooth for Mo-Ru and, as measured recently, for Kr isotopes [49].

ACKNOWLEDGMENTS

The authors thank Professor F. Iachello for valuable discussions. This work was performed in part with support by U.S. DOE Grant No. DE-FG-02-91ER-40608 and by a grant-in-aid for scientific research (No. 217368). The author K.N. acknowledges support by the JSPS. The author L.G. acknowledges support by the NSFC (Grant No. 11175252) and the President Fund of GUCAS. Part of the calculations were performed by using the RIKEN Integrated Cluster of Clusters (RICC) facility.

[1] R. Gilmore and D. H. Feng, Nucl. Phys. A **301**, 189 (1978).
[2] D. H. Feng, R. Gilmore, and S. R. Deans, Phys. Rev. C **23**, 1254 (1981).
[3] F. Iachello and S. Oss, J. Chem. Phys. **104**, 6956 (1996).
[4] D. Larese and F. Iachello, J. Mol. Struct. **1006**, 611 (2011).
[5] A. Bohr and B. R. Mottelson, *Nuclear Structure* (Benjamin, New York, 1969 and 1975), Vols. I and II.
[6] P. Cejnar, J. Jolie, and R. F. Casten, Rev. Mod. Phys. **82**, 2155 (2010).
[7] F. Iachello, Riv. Nuovo Cimento **34**, 617 (2011).
[8] P. Ring and P. Schuck, *The Nuclear Many-Body Problem* (Springer, Berlin, 1980).
[9] M. Bender, P.-H. Heenen, and P.-G. Reinhard, Rev. Mod. Phys. **75**, 121 (2003).
[10] T. Otsuka, M. Honma, T. Mizusaki, N. Shimizu, and Y. Utsuno, Prog. Part. Nucl. Phys. **47**, 319 (2001).
[11] Tomás R. Rodriguez and J. L. Egido, Phys. Lett. B **663**, 49 (2008).
[12] T. Nikšić, D. Vretenar, G. A. Lalazissis, and P. Ring, Phys. Rev. Lett. **99**, 092502 (2007).
[13] G. Gneuss, U. Mosel, and W. Greiner, Phys. Lett. B **30**, 397 (1969); **31**, 269 (1970).
[14] G. Gneuss and W. Greiner, Nucl. Phys. A **171**, 449 (1971).
[15] J. M. Eisenberg and W. Greiner, *Nuclear Models:Collective and Single-Particle Phenomena, Vol. 1 of Nuclear Theory*, 3rd ed (North-Holland, Amsterdam, 1987).
[16] F. Iachello and A. Arima, *The Interacting Boson Model* (Cambridge University Press, Cambridge, 1987).
[17] T. Otsuka, A. Arima, F. Iachello, and I. Talmi, Phys. Lett. B **76**, 139 (1978); T. Otsuka, A. Arima, and F. Iachello, Nucl. Phys. A **309**, 1 (1978).
[18] K. Nomura, N. Shimizu, and T. Otsuka, Phys. Rev. Lett. **101**, 142501 (2008).
[19] K. Nomura, N. Shimizu, and T. Otsuka, Phys. Rev. C **81**, 044307 (2010).
[20] K. Nomura, T. Otsuka, N. Shimizu, and L. Guo, Phys. Rev. C **83**, 041302(R) (2011).
[21] J. E. García-Ramos, J. M. Arias, J. Barea, and A. Frank, Phys. Rev. C **68**, 024307 (2003).
[22] M. A. Caprio and F. Iachello, Ann. Phys. (N.Y.) **318**, 454 (2005).
[23] A. E. L. Dieperink, O. Scholten, and F. Iachello, Phys. Rev. Lett. **44**, 1747 (1980); A. E. L. Dieperink and O. Scholten, Nucl. Phys. A **46**, 125 (1980); J. N. Ginocchio and M. W. Kirson, Phys. Rev. Lett. **44**, 1744 (1980); A. Bohr and B. R. Mottelson, Phys. Scr. **22**, 468 (1980).
[24] P. Bonche, H. Flocard, and P.-H. Heenen, Comput. Phys. Commun. **171**, 49 (2005).
[25] J. Bartel, P. Quentin, M. Brack, C. Guet, H.-B. Håkansson, Nucl. Phys. A **386**, 79 (1982).
[26] F. Iachello, Phys. Rev. Lett. **87**, 052502 (2001).
[27] NuDat 2.6, [http://www.nndc.bnl.gov/nudat2/].
[28] T. Otsuka and N. Yoshida, JAERI-M Report No. 85, 1985 (unpublished).
[29] D. Bonatsos, E. A. McCutchan, R. F. Casten, and R. J. Casperson, Phys. Rev. Lett. **100**, 142501 (2008).
[30] A. Artna-Cohen, Nucl. Data Sheets **79**, 1 (1996).
[31] C. W. Reich, Nucl. Data Sheets **110**, 2257 (2009).
[32] C. W. Reich, Nucl. Data Sheets **99**, 753 (2003).
[33] R. G. Helmer, Nucl. Data Sheets **101**, 325 (2004).
[34] C. W. Reich, Nucl. Data Sheets **105**, 557 (2005).
[35] B. Singh, Nucl. Data Sheets **95**, 995 (2002).
[36] C. W. Reich, Nucl. Data Sheets **108**, 1807 (2007).
[37] F. Iachello, N. V. Zamfir, and R. F. Casten, Phys. Rev. Lett. **81**, 1191 (1998).
[38] N. V. Zamfir, R. F. Casten, R. Krücken, C. W. Beausang, G. Cata-Danil, J. R. Cooper, Benyuan Liu, J. R. Novak, and C. J. Barton, in *Exotic nuclei and atomic masses (ENAM 98)*, edited by B. M. Sherrill, AIP Conf. Proc. No. 455 (AIP, New York, 1998), p. 614.
[39] R. Fossion, Rev. Mex. Fis. S **54**(3), 42 (2008).
[40] R. F. Casten, *Nuclear Structure from a Simple Perspective* (Oxford University Press, Oxford, 2000).
[41] A. H. Wapstra, G. Audi, and C. Thibault, Nucl. Phys. A **729**, 129 (2003).
[42] R. Fossion, C. De Coster, J. E. García-Ramos, T. Werner, and K. Heyde, Nucl. Phys. A **697**, 703 (2002).
[43] R. F. Casten and N. V. Zamfir, Phys. Rev. Lett. **87**, 052503 (2001).
[44] D. Tonev, A. Dewald, T. Klug, P. Petkov, J. Jolie, A. Fitzler, O. Möller, S. Heinze, P. von Brentano, and R. F. Casten, Phys. Rev. C **69**, 034334 (2004).
[45] A. Dewald, O. Möller, D. Tonev, A. Fitzler, B. Saha, K. Jessen, S. Heinze, A. Linnemann, J. Jolie, K. O. Zell, P. von Brentano, P. Petkov, R. F. Casten, M. Caprio, J. R. Cooper, R. Krücken, V. Zamfir, D. Bazzacco, S. Lunardi, C. Rossi Alvarez, F. Brandolini, C. Ur, G. de Angelis, D. R. Napoli, E. Farnea, N. Marginean, T. Martinez, and M. Axiotis, Eur. Phys. J. A **20**, 173 (2003).
[46] M. A. Caprio, N. V. Zamfir, R. F. Casten, C. J. Barton, C. W. Beausang, J. R. Cooper, A. A. Hecht, R. Krücken, H. Newman, J. R. Novak, N. Pietralla, A. Wolf, and K. E. Zyromski, Phys. Rev. C **66**, 054310 (2002).
[47] R. Krücken, B. Albanna, C. Bialik, R. F. Casten, J. R. Cooper, A. Dewald, N. V. Zamfir, C. J. Barton, C. W. Beausang, M. A. Caprio, A. A. Hecht, T. Klug, J. R. Novak, N. Pietralla, and P. von Brentano, Phys. Rev. Lett. **88**, 232501 (2002).
[48] O. Scholten, F. Iachello, and A. Arima, Ann. Phys. (N.Y.) **115**, 325 (1978).
[49] M. Albers *et al.*, Phys. Rev. Lett. **108**, 062701 (2012).